

Performance evaluation of high concentration photovoltaic cells cooled by microchannels heat sink with serpentine reentrant microchannels

Liang Chen^a, Daxiang Deng^{b,*}, Qixian Ma^b, Yingxue Yao^b, Xinhai Xu^b

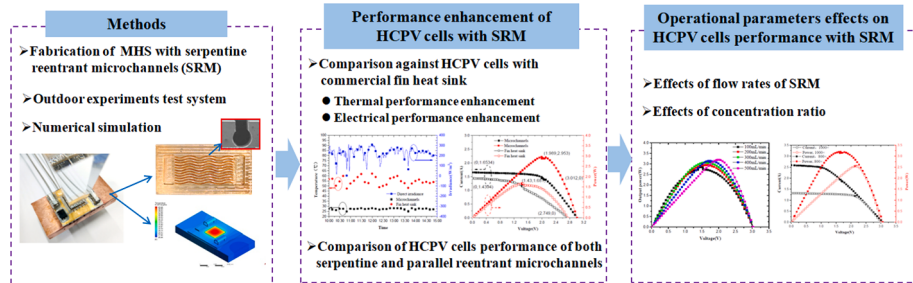
^a Department of Mechanical & Electrical Engineering, Xiamen University, Xiamen 361005, China

^b School of Mechanical Engineering and Automation, Harbin Institute of Technology, Shenzhen, Shenzhen 518055, China

HIGHLIGHTS

- Novel microchannel heat sink(MHS) with serpentine reentrant microchannels(SRM) were developed.
- MHS with SRM provided efficient cooling for high concentration photovoltaic (HCPV) cells.
- MHS with SRM reduced HCPV cell temperatures and enhanced temperature uniformity.
- MHS with SRM increased output power and improved electrical efficiencies of HCPV cells.
- Larger flow rate induce better thermal and electrical performance of HCPV cells with MHS with SR.

GRAPHICAL ABSTRACT



ARTICLE INFO

Keywords:

High concentration photovoltaic cell
Microchannels heat sink
Serpentine reentrant microchannels
Thermal performance

ABSTRACT

Efficient cooling is critical to reduce cell temperatures of high concentration photovoltaic (HCPV) cells to avoid the output electrical performance degradation and lifetime reduction. In this study, we develop a novel type of microchannel heat sink (MHS) with serpentine reentrant microchannels (SRM) for efficient cooling of HCPV cells. They feature serpentine flow passages with Ω -shaped cross-sectional configurations, which contribute to promote fluid mixing and disrupt the normal development of thermal boundary layers. Thus they are able to provide excellent heat transfer characteristics and highly efficient cooling performance. By the comparison of a fin heat sink, both numerical and outdoor experimental studies were comprehensively conducted to explore the enhancement feasibility of thermal and electrical performance of HCPV cells. Results showed that the SRM reduced the cell temperatures and enhanced the temperature uniformity of HCPV cell module considerably, i.e., it presented cell temperatures of 25–31°C, much smaller than that of 45–63°C of the fin heat sink. The temperature differences of HCPV cell modules were reduced to be less than 4.4°C. Besides, the output power increased by as high as 115%, and the electrical efficiency increased to 15–20% for the HCPV cell module with serpentine reentrant microchannels. Besides, the HCPV cell module with SRM was also found to induce smaller average cell temperatures and better electrical performance than a module with parallel reentrant microchannels (PRM). Moreover, the effects of flow rate and concentration ratio on the performance of HCPV cells with SRM were also assessed.

* Corresponding author.

E-mail address: dengdaxiang@hit.edu.cn (D. Deng).

1. Introduction

Concentration photovoltaic is an effective way to improve the overall photovoltaic(PV) efficiency and reduce the cost of photovoltaic systems by replacing the amount of expensive semiconductor material with cheap optical devices, such as lenses or mirrors [1–2]. Nevertheless, under high concentration ratios, heat accumulation into a small PV cell increases the PV cell temperatures remarkably. This results in output electrical performance degradation of HCPV cells and lifetime reduction due to mechanical failures and micro-cracks during long-term operation [3–4]. Therefore, it is critical to develop highly-efficient cooling methods to reduce the temperatures of HCPV systems. In recent decades, both passive and active cooling methods have been developed for HCPV devices. Passive cooling methods, such as natural convective air cooling of finned heat sinks [5–6], liquid immersion cooling [7–8], phase change materials [9–10], and heat pipe cooling [11], require no extra power consumption. Nevertheless, the natural convective air cooling of finned heat sinks, phase change materials and heat pipe cooling are unable to meet the increasing heat dissipation requirements of HCPV system due to their limited heat removal capacity, large heat sink size and high cost. For the liquid immersion cooling, the leak proof for the solar cells and complicated system may be problematic, and the corrosion problems may be also detrimental for the HCPV devices. On the contrary, in active cooling techniques, such as jet impingement [12–13], and microchannel heat sink [14–15] or hybrid jet impingement/microchannels [16], high heat removal capacity can be obtained by forced convection of fluid, and the temperature of HCPV devices can be remarkably reduced. Among the above active cooling techniques, the jet impingement and hybrid jet impingement/microchannels require large consumption of pumping power, and also have the disadvantages of non-uniform cooling performance [2].

Microchannel heat sink is an ideal candidate to address the cooling issue of HCPV devices due to its large specific surface area, compact structure and outstanding heat transfer performance [3,14,17,18]. High heat transfer rates can be achieved for microchannel heat sink, which is ideal for efficient cooling of HCPV system. Agrawal and Tiwari [19] developed a glazed hybrid microchannel solar cell thermal tile for efficient cooling. A 26.7% enhancement of the electrical efficiency was demonstrated compared to a single channel photovoltaic thermal module. Rahimi et al. [20] explored the heat transfer augmentation and output power improvement by a hybrid microchannel solar cell with rectangular microchannels of a 0.667 mm hydraulic diameter. Excellent cooling performance was found, and the maximum cell power was improved by above 30% compared to a conventional photovoltaic panel without microchannels. Yang et al. [21] designed a multi-layer manifold microchannel cooling system with rectangular configurations to effectively reduce the cell surface temperature and improve the temperature uniformity of concentration photovoltaic cells. The average temperature was controlled to be smaller than 37°C, and the surface temperature difference of the cell was smaller than 6.3°C under a 70 × concentration ratio in the indoor conditions. Ali et al. [22] numerically studied a four-compartment microchannel heat sink to cool high concentration photovoltaic module, and highlighted the importance of inlet and outlet orientation on the module temperature uniformity. Both parallel-flow and counter-flow operating conditions were studied, and the parallel-flow cases were found to induce smaller average module temperatures, whereas the counter-flow cases present more uniform temperature distribution. Besides, Radwan et al. [23] and Siyabi et al. [24] utilized double-layered microchannel heat sinks with rectangular configurations for the efficiently cooling of HCPV devices. Recently, Hong et al. [25] developed a two-phase radially expanding microchannel heat sink to cool solar-tracking high-concentration photovoltaic thermal hybrid system. Outdoor real-time sun tracking tests under a concentration ratio of 1070 suns indicated that the highest cell surface temperature was smaller than 110°C, and the maximum temperature difference was maintained to be smaller than 5 °C.

From the above literature review, previous studies on microchannel heat sink cooling systems for HCPV system have been focused on rectangular microchannels, despite that the flow passages can be modified to be of four-compartment [22], stepwise varying width [15], double-layered [23–24] or radially expanding [25] ones. Apart from the above flow passages, serpentine flow passages can also enhance convective heat transfer and improve the temperature uniformity along the flow direction. The serpentine channels introduce severe fluid mixing and acceleration along the flow passages, which periodically disrupt and redevelop thermal and hydraulic boundary layers. Therefore, heat transfer enhancement and more uniform temperature distributions can be obtained for the serpentine channels, which has been documented in repeated reports [26–28]. Sui et al. [26] found that the wavy serpentine microchannels with rectangular configurations were of much better heat transfer performance than that of straight baseline microchannels, and the pressure drop penalty of wavy microchannels could be much smaller than the heat transfer enhancement. Khoshvaght-Aliabadi et al. [27] obtained an about 200% heat transfer enhancement for the sinusoidal-wavy serpentine minichannels with rectangular configurations compared to straight counterpart in water-ethylene mixtures tests. The serpentine microchannels with rectangular configurations by Al-Neama et al. [28] also induced a 35% enhancement in heat transfer and a 19% reduction in total thermal resistance compared to straight rectangular microchannels.

Besides, conventional rectangular microchannels can be further enhanced by modifying flow passages or channel configurations to be of reentrant shaped cavities. Xia et al. [29–30] introduced triangular, offset fan-shaped and aligned fan-shaped reentrant cavities along the flow passages of rectangular microchannels. By the redevelopment of thermal and hydraulic boundary layers and vortices generation, significant convective heat transfer enhancement has been reached. Deng et al. [31] developed a type of parallel reentrant copper microchannels with unique Ω-shaped configurations. These reentrant microchannels were found to enhance heat transfer by up to 39%, and decrease the total thermal resistance by up to 22% compared to the conventional rectangular counterpart. The reentrant configurations contributed to flow separation by the throttling effects, the acceleration of fluid in the main flow and the intensification of fluid mixing, which was promising for heat transfer enhancement.

From the above literature review, the serpentine microchannels and reentrant configurations both contribute to enhanced heat transfer performance. Nevertheless, previous serpentine microchannels were all focused on rectangular configurations, and the reentrant cavities were only introduced to parallel rectangular microchannels to date. Serpentine reentrant microchannels, which combine both merits of serpentine flow passages and reentrant microchannels, are believed to provide excellent heat transfer characteristics and highly efficient cooling performance. To this aim, we in this study developed a novel type of microchannel heat sink with serpentine reentrant microchannels(SRM) for efficient cooling of HCPV cells. The serpentine reentrant microchannels were fabricated and integrated with HCPV cells for the first time. By the comparison of a commercial fin heat sink with natural convection cooling, both numerical and outdoor experimental studies were conducted to explore the enhancement feasibility of thermal and electrical performance of the MHS with serpentine reentrant microchannels, which are described in Section 2 and Section 3. Besides, the HCPV cell module with SRM was also compared to a module with parallel reentrant microchannels (PRM). The above builds of the first part of this paper, and the results are presented in Section 4.2. Moreover, the effects of inlet flow rate and concentration ratio on the thermal and electrical performance of the HCPV cells with SRM were also evaluated to explore their performance comprehensively, which are presented in Section 4.3 and 4.4. Finally, the main conclusions are summarized in Section 5.

2. Experiments

2.1. Design and fabrication of microchannels heat sink with serpentine reentrant microchannels

The schematic of serpentine reentrant microchannels is shown in Fig. 1(a). The serpentine reentrant microchannels are designed to be of Ω -shaped configurations, i.e., large circular cavities inside and exit narrow slot upside. The dimensions of reentrant microchannels are shown in Fig. 1(a). The hydraulic diameter (D_h) of reentrant microchannels can be calculated to be 814 μm . The wave-length and wave-amplitude of the serpentine reentrant microchannels are 10 mm and 1.5 mm, respectively. A total of 11 serpentine reentrant microchannels are prepared, and the spacing between two microchannels is 1.3 mm. Before and after the serpentine reentrant microchannels, two inlet and outlet manifolds are prepared to store the liquid, and the dimensions are 15 mm \times 6 mm \times 1.5 mm in width, length and depth, respectively.

The serpentine microchannels sample is fabricated on a pure copper plate of 50 mm in length, 25 mm in width and 4 mm in depth by micro-milling process. The picture and microscopic images of the fabricated microchannels sample are shown in Fig. 1(b). After that, the microchannels plate is integrated with a 3.5 mm plain copper plate with the same width and length, and soldered together by vacuum diffusion welding to form the microchannel heat sink.

For comparison, conventional parallel reentrant microchannels (PRM) with identical Ω -shaped configurations are also prepared for comparison, in which 11 parallel reentrant microchannels are prepared in the microchannel sample, as shown in Fig. 2. All the other geometric sizes of the parallel reentrant microchannels are identical to the

serpentine reentrant microchannels.

2.2. Concentration photovoltaic cell cooling module

The GaInP/GaInAs/Ge triple-junction solar cells are used to build of the HCPV cell module, which are provided by Tianjin Lantian Solar Technology Co., Ltd.. The triple-junction solar cells are of 10.8 mm in length, 10.1 mm in width, and 195 μm in thickness. The effective cell aperture area is 99 mm². The specifications of the triple-junction solar cells in the standard condition AM1.5G in the laboratory are listed in Table 1. The package of the PV cell is shown in Fig. 3, in which the solar cell is attached to a high thermal conductivity ceramic substrate. The package is of 28 mm in length, 24 mm in width, and 2 mm in thickness.

The schematic of HCPV cell cooling module is shown in Fig. 4. The package of PV cell is stacked to the center of upper surface of micro-channel heat sink device by thermal grease. To improve the incident light distribution uniformity and ensure the complete absorption of concentrated sunlight, a secondary prismatic glass concentrator is attached on the top of the PV cell by the highly transparent optical glue. The prismatic glass concentrator is of 10 mm \times 10 mm on the bottom, and 21 mm \times 21 mm on the top, and a height of 43 mm. The picture of HCPV cell module with microchannel heat sinks are shown in Fig. 5(a).

As common HCPV cells are cooled by fin heat sinks in the commercial industry, we also utilize a commercial aluminum fin heat sink as a benchmark to evaluate the performance enhancement feasibility of the MHS with serpentine reentrant microchannels, as shown in Fig. 5(b). The overall dimension of the fin heat sink is 77 mm \times 75 mm \times 25 mm. The total surface area of the air cooled heat sink is approximately 3.9 cm².

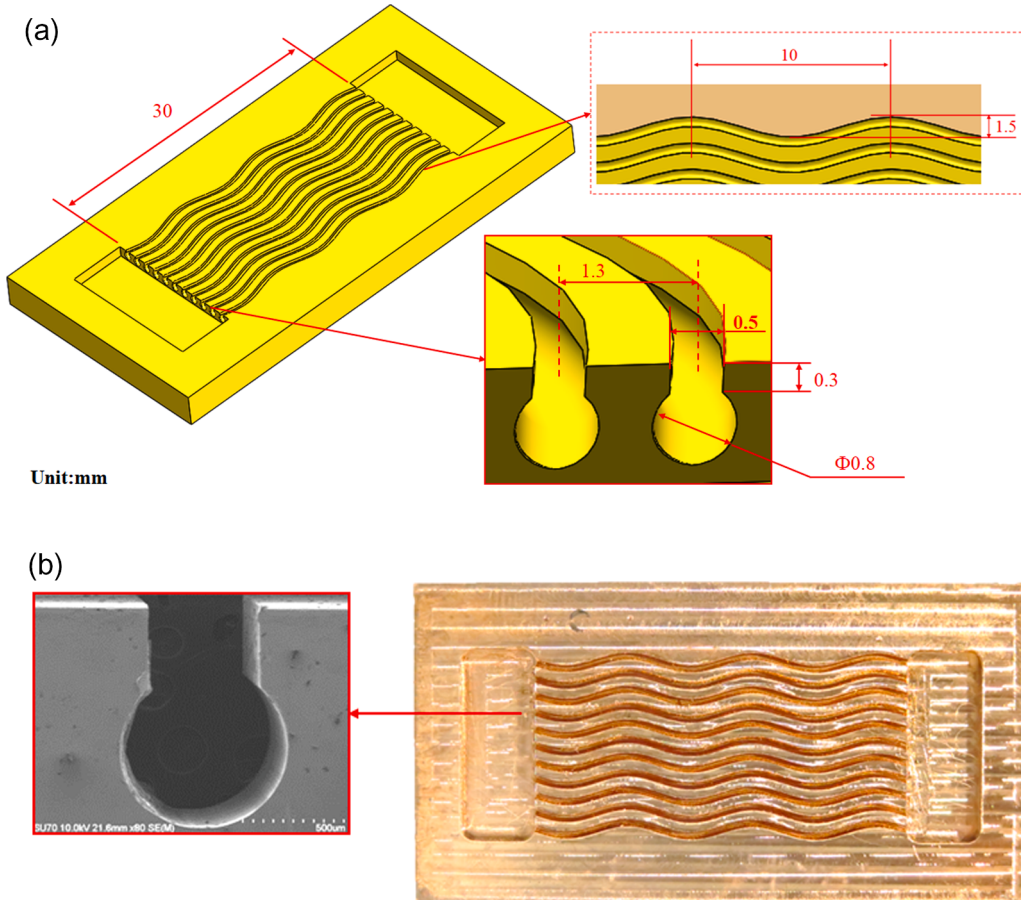


Fig. 1. Microchannel heat sinks with serpentine reentrant microchannels: (a) Schematic and geometric design of serpentine reentrant microchannels; (b) Picture and SEM figure of the serpentine reentrant microchannels.

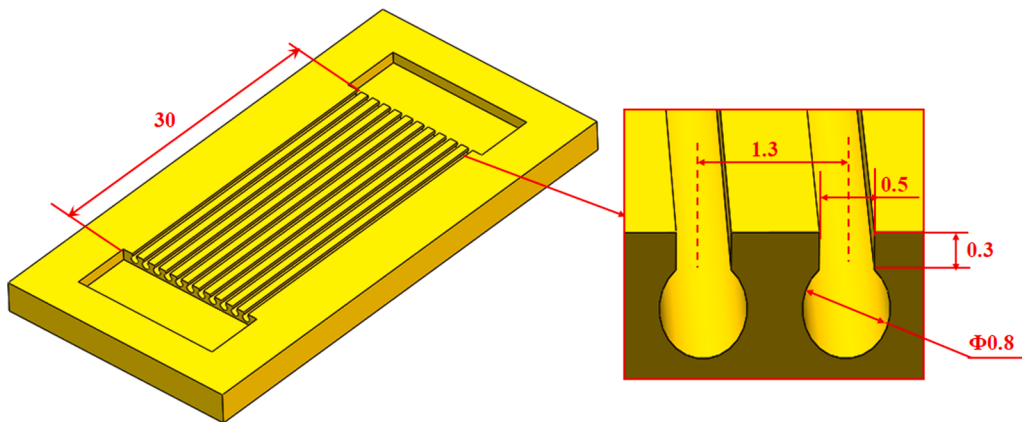


Fig. 2. Schematic of conventional parallel reentrant microchannels.

Table 1
Specifications of the InGaP/InGaAs/Ge triple-junction CPV cells.

Parameters	Value
Concentration ratio	500
V _{oc} (V)	3.24
I _{sc} (A)	6.97
P _{max} (W)	19.85
FF(%)	88
Efficiency(%)	40.1

2.3. Outdoor experiment test system

The schematic of the outdoor HCPV test system is shown in Fig. 6(a), and the picture of the outdoor system is shown in Fig. 6(b). It mainly consists of six parts, i.e., concentration components, solar tracking components, electrical monitoring components, temperature monitoring components, environmental data collection components, and cooling circulation loop. The concentration components are mainly composed of a point-focus Fresnel lens and the secondary concentrator. The Fresnel lens is made of polymethyl methacrylate (PMMA), and its size is 355 mm × 355 mm × 3 mm. The focal distances of the optical concentrator are adjusted to obtain different concentration ratios of 1000 × and 800 × based on the calculation methods of Yin et al. [32]. In

solar tracking components, a two-axes sun tracer is utilized to track the sun to keep the incident sun rays perpendicular to the Fresnel lens. In the electrical and temperature monitoring components, an electronic load (M9140) is connected to the PV cell to monitor the I-V curves. K-type thermocouples are utilized to measure the temperature data of the triple-junction solar cells and the environment. The thermocouples are set on the backside of the PV cell package. Fig. 7 shows the thermocouples distributions of the PV modules with both microchannels and fin heat sinks, in which T3 is located in the middle of the heat sink, and the rest thermocouples are symmetrically arranged. The distance between each two adjacent thermocouples is 5 mm. The environmental data collection components consist of several sensors to record the wind velocity and direction, humidity, direct and total solar irradiances. In the cooling circulation loop, the water is pumped by a magnetically coupled gear pump. Then it flows through a low constant temperature bath and a flowmeter, and enters the microchannels. After the heat exchange in microchannels heat sinks, the water goes back to the water tank. All the data are collected by a data acquisition system with Agilent 34970A. In this study, the deionized water is used as the coolant. The outdoor experiments are conducted in Xiamen University in Xiamen (E118.08° / N24.48°), Fujian Province, China.

In this study, the HCPV cell cooling modules with microchannel heat sink and fin heat sink are simultaneously studied in identical ambient conditions, i.e., the flow rate of 500 mL/min and concentration ratio of 1000 × . Besides, to explore the performance of the HCPV cell module

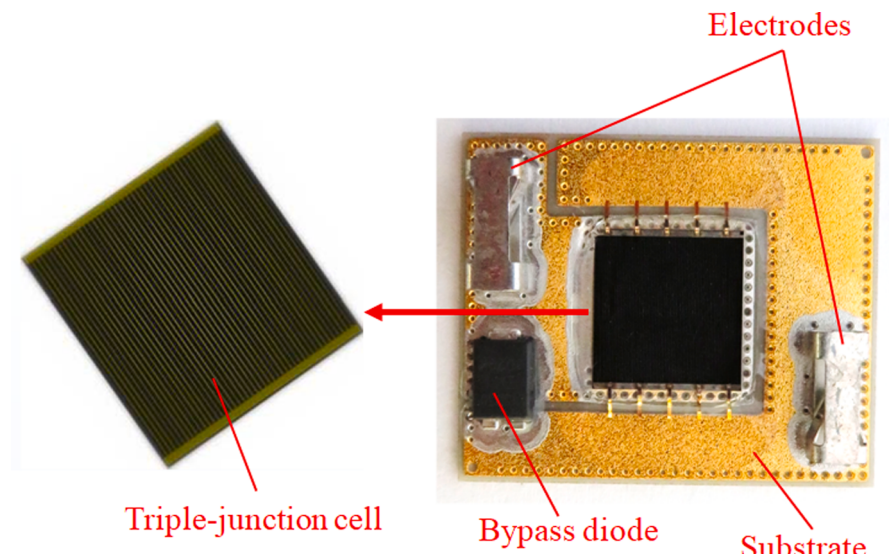


Fig. 3. Picture of the package of the triple-junction CPV cell.

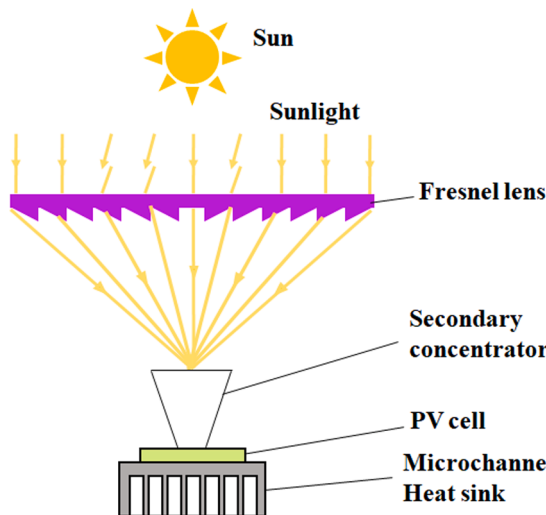


Fig. 4. Schematic of high concentration photovoltaic cell cooling module.

with serpentine reentrant microchannels comprehensively, five inlet flow rates of the microchannels are tested for the module with SRM, i.e., 100, 200, 300, 400, and 500 mL/min in the concentration ratio of 1000 \times . The inlet temperature is maintained to be 25°C. Moreover, another concentration ratio of 800 \times was also prepared for the module with SRM. After 5 min of stable operation of each test, the output characteristics of the CPV cell are recorded at 1 min interval.

2.4. Data reduction

The output electrical performance of HCPV cell can be determined by the I-V and P-V curves. The maximum output power (P_{max}) of the HCPV cells can be obtained as follows:

$$P_{max} = I_m V_m \quad (1)$$

where I_m and V_m is the current and voltage on the maximum power point.

The input power (P_{in}) of the HCPV cells from the solar energy can be calculated as follows,

$$P_{in} = C_r G_d A_t \eta_1 \eta_2 \quad (2)$$

where C_r , G_d , A_t , η_1 and η_2 are the concentration ratio, direct solar irradiance(DNI), the area of the HCPV cells, the transmissivity efficiency of Fresnel lens and the transmissivity efficiency of the secondary concentrator, respectively.

The electrical efficiency(η_e) of the HCPV cells can be obtained as follows,

$$\eta_e = \frac{P_{max}}{P_{in}} = \frac{I_m V_m}{C_r G_d A_t \eta_1 \eta_2} \quad (3)$$

The average temperature on the bottom of the HCPV cells (T_b) is used to evaluate the temperature of the HCPV cells, which can be determined as follows,

$$T_b = \frac{1}{5} \sum_{i=1}^5 T_i \quad (5)$$

where T_i is the thermocouple measurement on the bottom of the CPV cells.

Uncertainties of the calculated parameters can be determined by the standard error analysis method [33],

$$U_z = \sqrt{\sum_{i=1}^n \left[\frac{\partial Z}{\partial x_i} U_{x_i} \right]^2} \quad (6)$$

where U_z is the uncertainty of Z parameter, x_i is the measured parameters, U_{x_i} is the uncertainty of x_i parameter. The detailed uncertainties of the parameters are listed in Table 2.

3. Numerical simulation

3.1. Physical model

A numerical 3D conjugate heat transfer simulation is carried out for the HCPV cell cooling module. Fig. 8(a) shows the model of HCPV cell module, which consists of a cell layer (GaInP-GaInAs-Ge, 10 × 10 mm²), upper copper layer, Al₂O₃-Ceramic layer, lower copper layer, and microchannel heat sink from the top to the bottom. It also consists of a by-pass diode and two electrical terminals. The dimensions of the CPV cooling module are listed in Table 3, and the thermophysical properties of each layer of the module are listed in Table 4.

The amount of heat (q_s) that cannot be converted to electricity by the solar cells can be calculated as follows,

$$q_s = P_{in}(1 - \eta_e) \quad (7)$$

The electrical efficiency can be calculated as follows [34–35],

$$\eta_e = \eta_{ref} - \beta \cdot (T_{cell} - T_{ref}) \quad (8)$$

where $\beta = 0.047\%/\text{K}$ is the thermal coefficient; $\eta_{ref} = 41.2\%$ is the typical electrical efficiency at the reference temperature $T_{ref} = 298.15\text{ K}$ under a concentration ratio of 1000 in direct normal irradiance of 1000 W/m².

The amount of heat by solar cell are dissipated mainly by the heat exchange of microchannel heat sink (q_m), and partially dissipated due to convection and radiation,

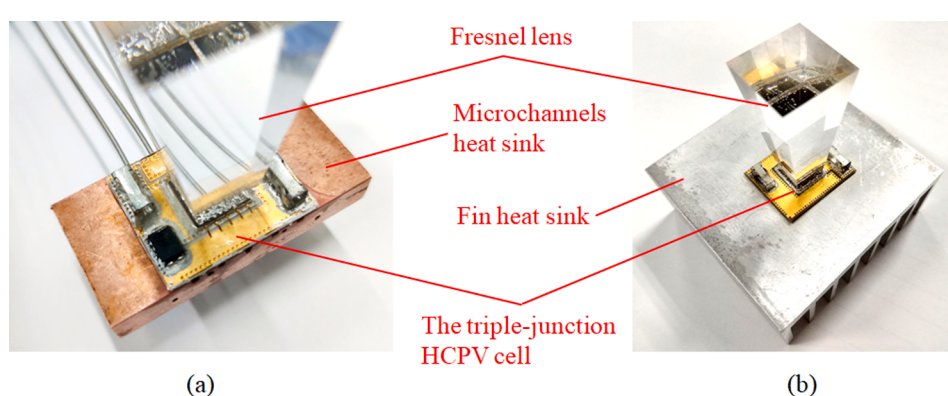


Fig. 5. The HCPV cooling module with different cooling methods:(a)microchannels heat sink; (b)fin heat sink.

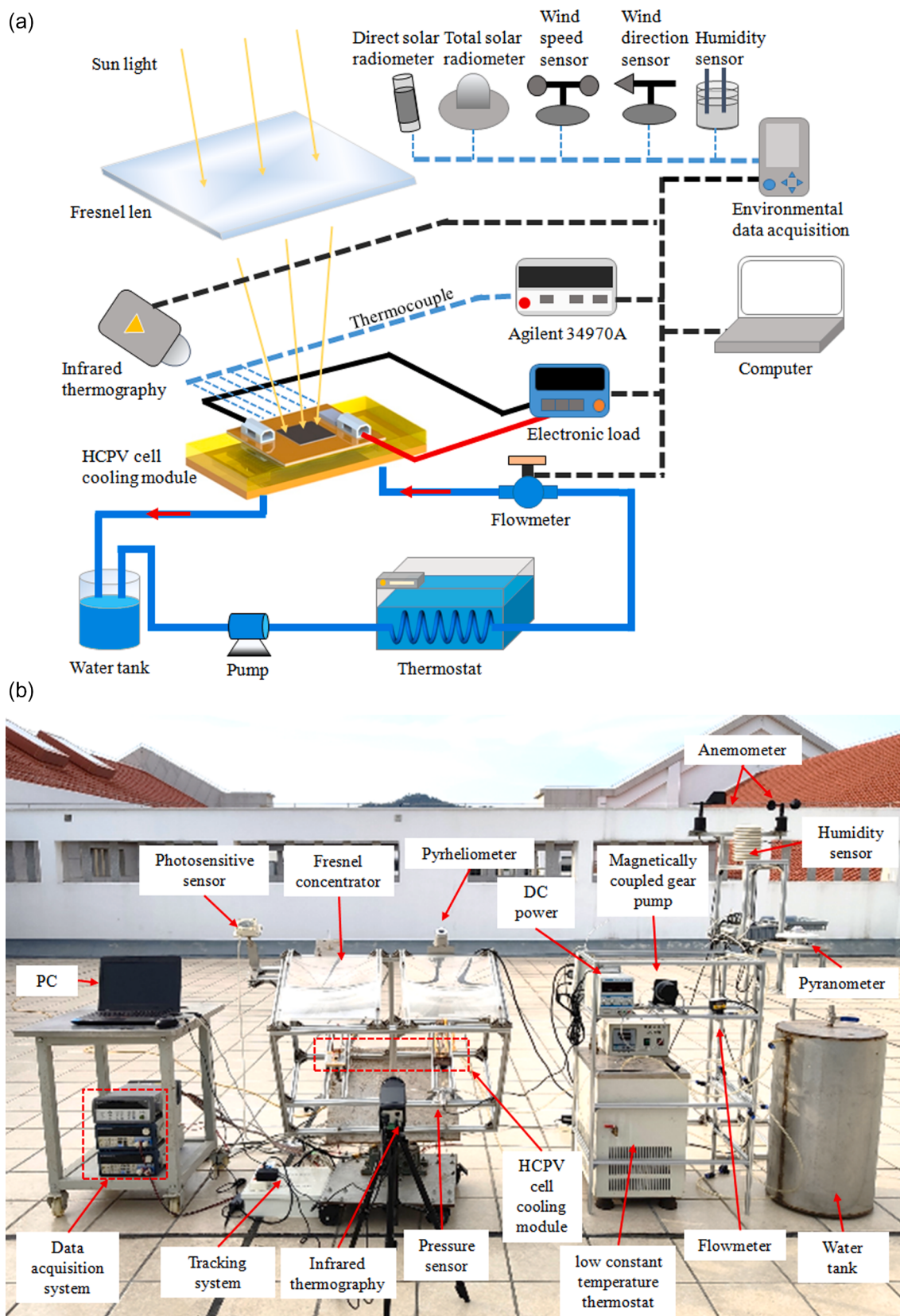


Fig. 6. Outdoor HCPV test system: (a)Schematic of test system; (b)Picture of test system.

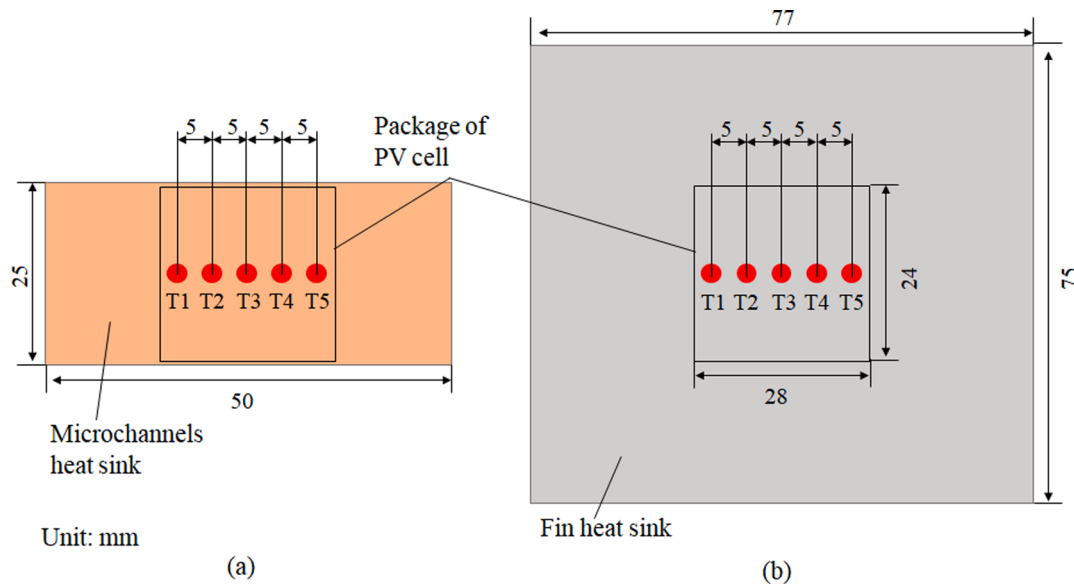


Fig. 7. Thermocouples distributions of the PV modules with both heat sinks: (a) microchannel heat sink; (b) Fin heat sink.

Table 2
Uncertainties in variables.

Parameters	Uncertainties
Temperature	0.3°C
Flow rate	2%
Voltage	0.015%
Current	0.05%
Output power	0.587%
Solar irradiance	1%
Length(mm)	0.1
Humidity(%RH)	±4%(<80%) ±8%(>80%)
Wind velocity	0.01 m/s
Wind direction	3°
η_e	5.6%

$$q_s = q_m + q_c + q_r \quad (9)$$

where the heat loss by convection(q_c) and radiation(q_r) from the surfaces of the CPV assembly can be calculated as follows,

$$q_c = A_c \cdot h_c \cdot (T_w - T_a) \quad (10)$$

$$q_r = \varepsilon \cdot \sigma \cdot A_r \cdot (T_w^4 - T_a^4) \quad (11)$$

where h_c is convection heat transfer coefficient by wind(W/m²·K), A_c is the convection area, T_w is the average surface temperature, and T_a is the ambient temperature. ε is the emissivity; σ is Stefan–Boltzmann constant; A_r is the radiation area;

For the GaInP/GaInAs/Ge triple-junction solar cells, the convection loss can be obtained as the function of Nusselt number (Nu),

$$h_c = \frac{Nu \cdot k_f}{l} \quad (12)$$

where the k_f is the thermal conductivity of wind, l is the characteristic dimension.

The Nu can be calculated by the following empirical formula during the forced convection of wind on horizontal plates [36],

$$Nu = 0.664 Re_l^{1/2} Pr^{1/3} \quad (13)$$

where Pr is the Prandtl number, Re_l is the Reynolds number over the entire length of the plate. Eq. (13) is in good agreement with previous

experimental results when Re_l is less than 5×10^5 , as pointed out in Ref. [36]. The Re_l can be calculated as follows,

$$Re_l = \frac{\rho u_{wind} l}{\mu} \quad (14)$$

where u_{wind} is the wind velocity; ρ is the air density; μ is the kinetic viscosity of air.

In the microchannel heat sinks, the following assumptions are made to simplify the thermal analysis [37]: (1) The flow is incompressible and in steady-state; (2) The effect of gravity force is negligible; (3) Radiation heat transfer is negligible; (4) All solid walls of the channel are no slip and impermeable.

The governing equations consist of the continuity equation, the momentum equation and the energy equation for the liquid, which are listed respectively as follows:

$$\nabla \cdot (\rho \vec{V}) = 0 \quad (15)$$

$$\vec{V} \cdot \nabla (\rho \vec{V}) = - \nabla P + \nabla \cdot (\mu \nabla \vec{V}) \quad (16)$$

$$\vec{V} \cdot \nabla (\rho C_f T_f) = \nabla \cdot (k_f \nabla T_f) \quad (17)$$

The boundary conditions are assumed as follows: (1) The applied concentration ratio is 1000×; (2) The ambient temperatures is set to be 25 °C; (3) Uniform velocity and fixed fluid temperature of 25 °C are set at the inlet of microchannel heat sink; (4) The pressure outlet is selected, and the pressure at the outlet is assumed to be atmospheric. (5) The walls between the solid and fluid domains are set as fluid–solid coupling interfaces with a continuity of heat flux and temperature, and no-slip boundary condition is set.

Commercial software ANSYS Fluent 16.0[38] is used to simulate the coupled heat transfer between solid and fluid. The HCPV cooling module with microchannels is created in Solidworks, then it is imported into ICEM for meshing. The standard SIMPLE algorithm is used to realize the coupling of pressure field and velocity fields. The pressure equation is solved using a standard scheme, and the momentum and energy equations are discretized via a second-order, upwind scheme. Fig. 8(b) shows the grid meshing of the 3D model, in which non-uniform grids are utilized in the computational domain. Numerical solutions are assumed to be converged when the residuals of the mass and momentum equations reached 10^{-4} and the residual values of the energy equations reach 10^{-6} .

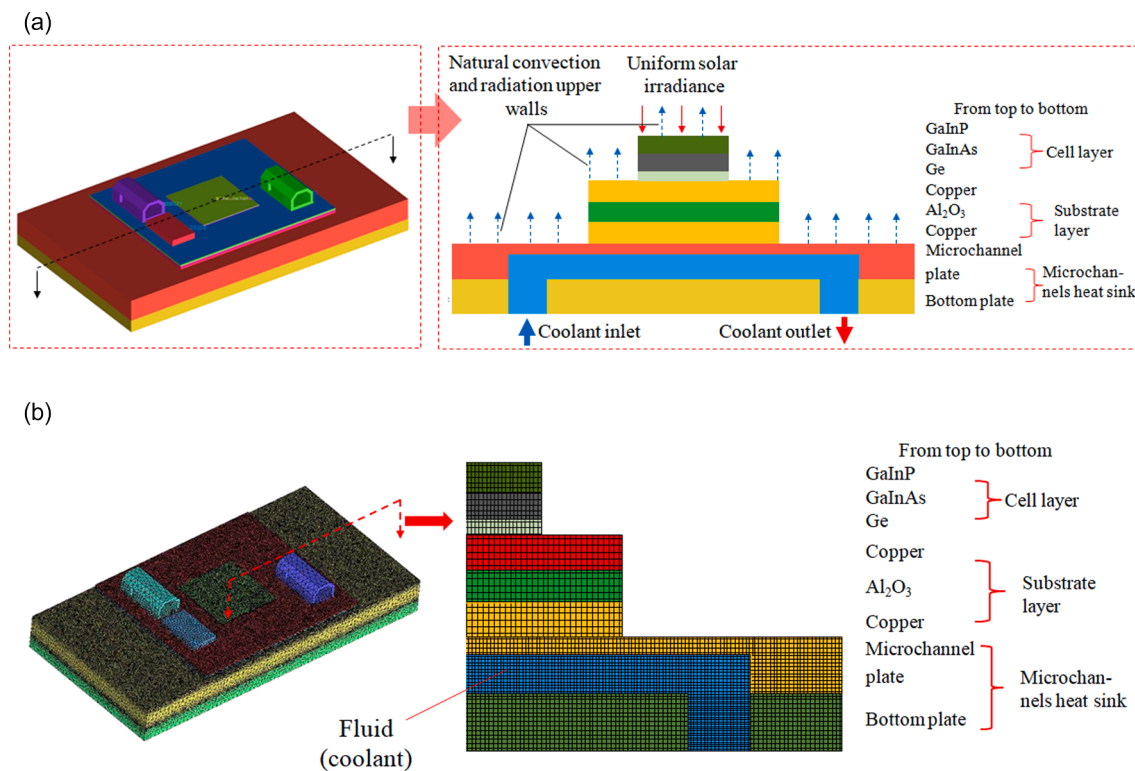


Fig. 8. Schematic diagram of the CPV cooling module in numerical simulation: (a) Schematic of the CPV cooling module; (b) Grid structures of the CPV cooling module.

Table 3
Dimensions of CPV cooling module in the simulations.

Material	Dimension(mm)	Thickness(mm)
GaInP	10 × 10	0.066
GaInAs	10 × 10	0.067
Ge	10 × 10	0.067
Upper copper	27 × 25	0.250
Al ₂ O ₃ -Ceramic	29 × 27	0.320
Lower copper	29 × 27	0.250
Microchannel heat sink	50 × 50	7.5

Table 4
The thermophysical properties of CPV cells.

Material	Density (Kg/m ³)	Thermal conductivity (W/(m·K))	Specific heat (J/(Kg·K))
GaInP	5300	73	73
GaInAs	5500	5	300
Ge	5323	60	310
Electrical terminals	2700	160	900
Copper	8700	400	385
Al ₂ O ₃ ceramic	3700	20	880
by-pass diodes	2329	130	700

3.2. Grid independence test

To make sure that the solution is not influenced by grid sizes of simulation, the sensitivity analysis of grids of the cooling module are performed. The pressure drop from the inlet to the outlet of the heat sink is utilized to study the grid dependence. Four non-uniform grid systems with different grids number are explored with 0.517×10^7 , 1.328×10^7 , 2.442×10^7 and 3.135×10^7 grids, respectively. The deviation of pressure drop using 0.517×10^7 , 1.328×10^7 , and 2.442×10^7 grids from that using 3.135×10^7 grids are 5.7%, 4.1%, and 1.7%, respectively, as shown in Table 5. It suggests that excessive refinement of grids

showed no improvement of the computational results. Therefore, the grids number with 3.135×10^7 was finally chosen in this simulation study.

4. Results and discussion

4.1. Validation of numerical simulation results

In order to validate the numerical simulation results, the temperature distributions on the bottom of the HCPV cell module with serpentine reentrant microchannels in numerical simulation in the flow rate of 300 mL/min are compared to the outdoor experiment results, as shown in Fig. 9. Reasonably good agreement is achieved between the numerical simulation and experiments results, i.e., the deviations of temperatures in different thermocouple locations are within the range of 4.0–7.9%. The deviations may result from the assumptions in the numerical part, such as negligible heat loss from the top of the cell to the surrounding environment by the radiation. Therefore, numerical simulations can be accepted reasonably to be validated by the experiments.

4.2. Enhancement of thermal and electrical performance by microchannels heat sink with serpentine reentrant microchannels

4.2.1. Comparison against HCPV cells with fin heat sink

Fig. 10 shows the thermal performance of the HCPV cells in outdoor experiments in microchannels heat sink with serpentine reentrant

Table 5
Grid independence analysis results.

Grids number × 10 ⁷	ΔP(kPa)	Deviation of ΔP
0.517	3.711	5.7%
1.328	3.774	4.1%
2.442	3.867	1.7%
3.135	3.933	—

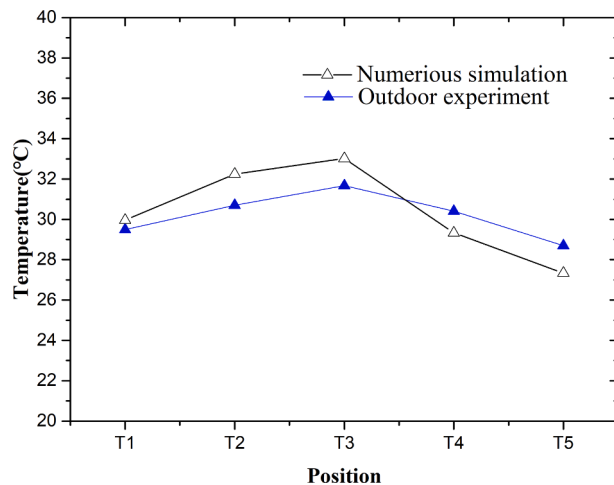


Fig. 9. Comparison of temperature distribution on the bottom of the HCPV cooling module in both numerical simulation and outdoor experiment.

microchannels and fin heat sink cooling conditions. The tests were conducted during 10:00 to 15:00, Oct. 11, 2019, in which the wind velocity was within 2.2 m/s, the humidity was 49%-64.4%, and the inlet flow rate was 500 mL/min. The average temperature of the HCPV cell module

with different cooling heat sinks are shown in Fig.10(a), and the temperature distributions HCPV cells between microchannels heat sink and fin heat sink cooling conditions are shown in Fig.10(c) and (d), respectively.

It can be noted that the temperatures of HCPV cell module with serpentine reentrant microchannels fluctuated in the small range of 25-31°C, whereas the temperature of HCPV cell module with fin heat sink fluctuated in much higher temperatures of 45-63°C. The fluctuation of wall temperatures of the HCPV cell module were generally consistent with the changes of the direct solar irradiance, as shown in Fig. 10(a). This can be related to the fact that the heat input to the cell was increased when the direct solar irradiance increased [39]. Besides, the temperature differences HCPV cell modules in microchannels heat sink and fin heat sink cooling conditions are shown in Fig. 10(b). The maximum temperature difference of HCPV cell module with microchannel heat sinks was less than 4.4°C, and most of them were within 1-3°C. On the other hand, the maximum temperature difference of the HCPV cell module with fin heat sink was up to 8.1°C, and most of them were within 3-7°C. The above difference can be linked to that the excellent heat transfer performance of microchannels heat sinks with serpentine reentrant microchannels. By the large heat transfer area and excellent heat exchange between the microchannels and liquid, the heat of HCPV cell could be dissipated quickly by the microchannels heat sinks. Thus the HCPV cell module can be maintained to be efficiently cooled, and its temperature distributions can be maintained to be much

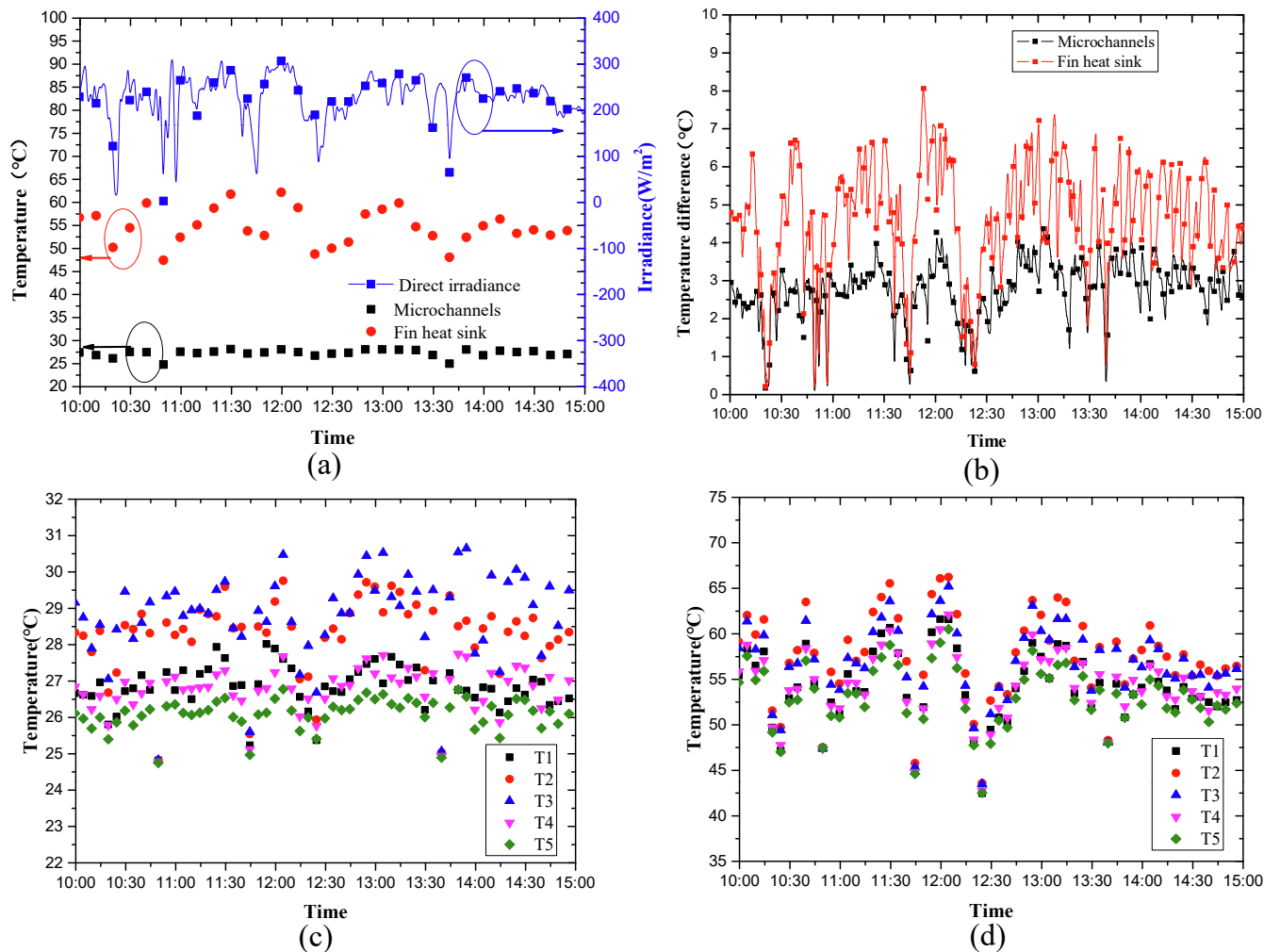


Fig. 10. Temperatures of both HCPV cell modules with microchannels heat sink with serpentine reentrant microchannels and fin heat sink: (a)Comparison of average temperature of HCPV cells; (b)Comparison of temperature difference of HCPV cells; (c)Temperature distribution of HCVP cell module with microchannels heat sink; (d) Temperature distribution of HCVP cell module with fin heat sink.

lower than that of fin heat sink cooling conditions. Moreover, the wall temperature uniformity can be also improved for microchannel heat sink cooling system. Fig. 11 illustrates the temperature profiles of both HCPV cell module with microchannels heat sinks and fin heat sinks in simulation results. It can be clearly noted that the HCPV cell temperature can be remarkably reduced by the microchannels heat sink with serpentine reentrant microchannels.

The heat transfer process in microchannels heat sinks with serpentine reentrant microchannels are shown in Fig. 12 by numerical simulations. Fig. 12(a) shows the temperature distribution in the cross-section of the HCPV cooling module with microchannels heat sink. The heat generated from the HCPV cell was first transferred to the microchannels base plate, and was then dissipated by microchannels via the convective heat transfer between the microchannel walls and the liquid in the reentrant microchannels. The unique reentrant microchannels facilitate the acceleration of fluid particles and the intensification of fluid mixing in the unique reentrant configurations, which has been pointed out in our previous studies [31]. Moreover, the normal developments of thermal and hydraulic boundary layers in microchannels were disrupted by serpentine flow passages. Thus good heat transfer performance can be maintained along the flow channels. Fig. 12(b) depicts the velocity vectors of three parts in the serpentine microchannels. In the serpentine zones, the fluid tended to flow in a sinusoidal-wavy flow direction, which would promote the mixing of hot and cold fluid, and improve the temperature uniformity [27]. At the same time, the thermal boundary layers tended to be thinner in the serpentine zones (Fig. 12(c)), which tended to promote the convective heat exchange process. Therefore, much smaller wall temperatures and more uniform temperatures distributions of HCPV cell module can be maintained for microchannel heat sink cooling systems with serpentine reentrant microchannels.

The output electrical performance of HCPV cell modules with both heat sink cooling conditions is shown in Fig. 13. From Fig. 13(a), the output power of HCPV cell module with microchannels heat sink was generally within 2.0–3.2 W, much larger than those of 1.4–1.6 W of fin heat sink counterpart. A maximum 115% increment in the output power was obtained for the microchannels heat sink cooling system. Besides, the electrical efficiency of HCPV cell module with microchannels heat sink was much larger than the fin heat sink counterpart, as shown in Fig. 13(b), i.e., the HCPV cell module with microchannels heat sink generally presented electrical efficiencies of 15–20%, whereas the fin heat sink counterpart were of electrical efficiencies of 9–12%. Fig. 13(c) illustrates typical I-V and P-V curves of solar cell at 11:30am at noon. It was found that the maximum output power (P_{max}), short circuit current (I_{sc}) and open voltage (V_{oc}) of the HCPV cell with microchannels heat sinks were 2.953 W, 1.6534A and 3.012 V, respectively. On the other hand, these were only 1.681 W, 1.4394A and 2.749 V for fin heat sink

cooling system. Therefore, an increment as high as 76% in the output power can be obtained by the microchannel heat sinks. The above enhancement can be closely linked to that the microchannel heat sink produced much better cooling performance and decrease the cell temperature considerably. As the output power and electrical conversion efficiency declines when the cell temperature increased [40], the enhanced cooling performance by microchannel heat sinks with serpentine reentrant microchannels contributed to much better output electrical performance of the triple-junction solar cell. Therefore, the microchannel heat sinks with serpentine reentrant microchannels contributed to both favorable thermal and output electrical performance of the HCPV cell module.

4.2.2. Comparison of the HCPV cells performance of both serpentine and parallel reentrant microchannels

Fig. 14 shows the comparison of thermal and electrical performance of HCPV cell modules cooled by both serpentine and parallel reentrant microchannels, in which both modules were tested in the flow rate of 500 mL/min and concentration ratio of 1000 × . The maximum and average cell temperatures of HCPV cell module with SRM were a little smaller than that with PRM as shown in Fig. 14(a). This can be attributed to that the serpentine flow passages contributed to the more intense fluid mixing inside the microchannels, and also periodically disrupt the common development of thermal and hydraulic boundary layers along the microchannels. The heat exchange between the microchannels walls and liquid was thus enhanced. Therefore, the SRM reduced the cell temperatures of HCPV cell module in general. The typical P-V and I-V curves of the HCPV cell in Fig. 14(b) indicated that the output power of the SRM was larger than that of PRM, i.e., the SRM induced the maximum output power of 2.842 W, about 7% larger than the one of PRM. This can be related to that the enhanced heat transfer performance by serpentine reentrant microchannels contributed to better output electrical performance of the triple-junction solar cell. Therefore, the serpentine reentrant microchannels showed its favorable performance in the cooling of HCPV cell module compared to the parallel reentrant microchannels.

4.3. Effect of flow rate on the performance of HCPV cell module with serpentine reentrant microchannels

Fig. 15(a) shows the average temperatures of HCPV cell module with serpentine reentrant microchannels at five different flow rates of 100–500 mL/min. A monotonic decreasing trend of the PV cell temperature can be noted with the increase in flow rates. This can be due to that more heat of PV cell was dissipated by microchannels heat sinks with the increase in flow rates, as the convective heat transfer between the reentrant microchannel and liquid enhanced when the flow rate

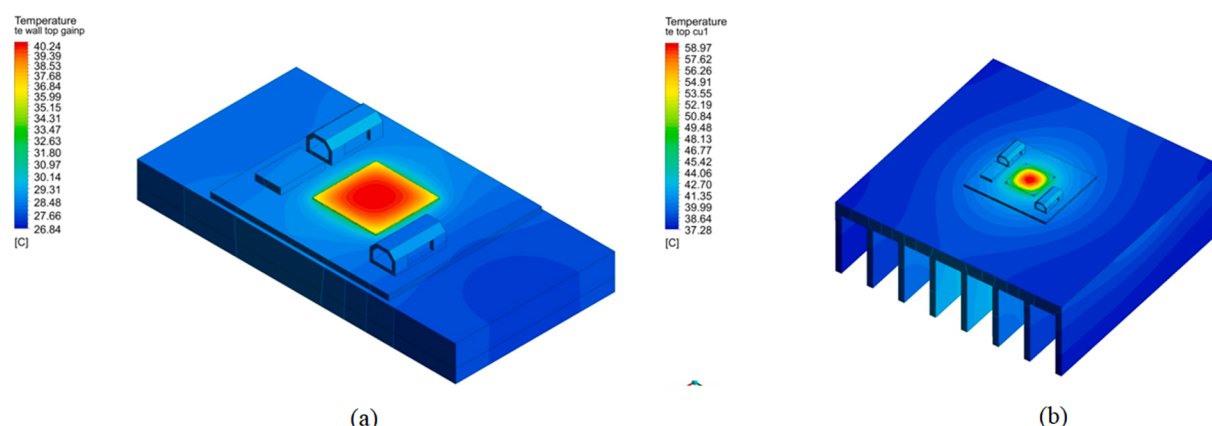


Fig. 11. Comparison of temperature distribution of the HCPV cell module with: (a) microchannel heat sinks with serpentine reentrant microchannels; (b) fin heat sinks.

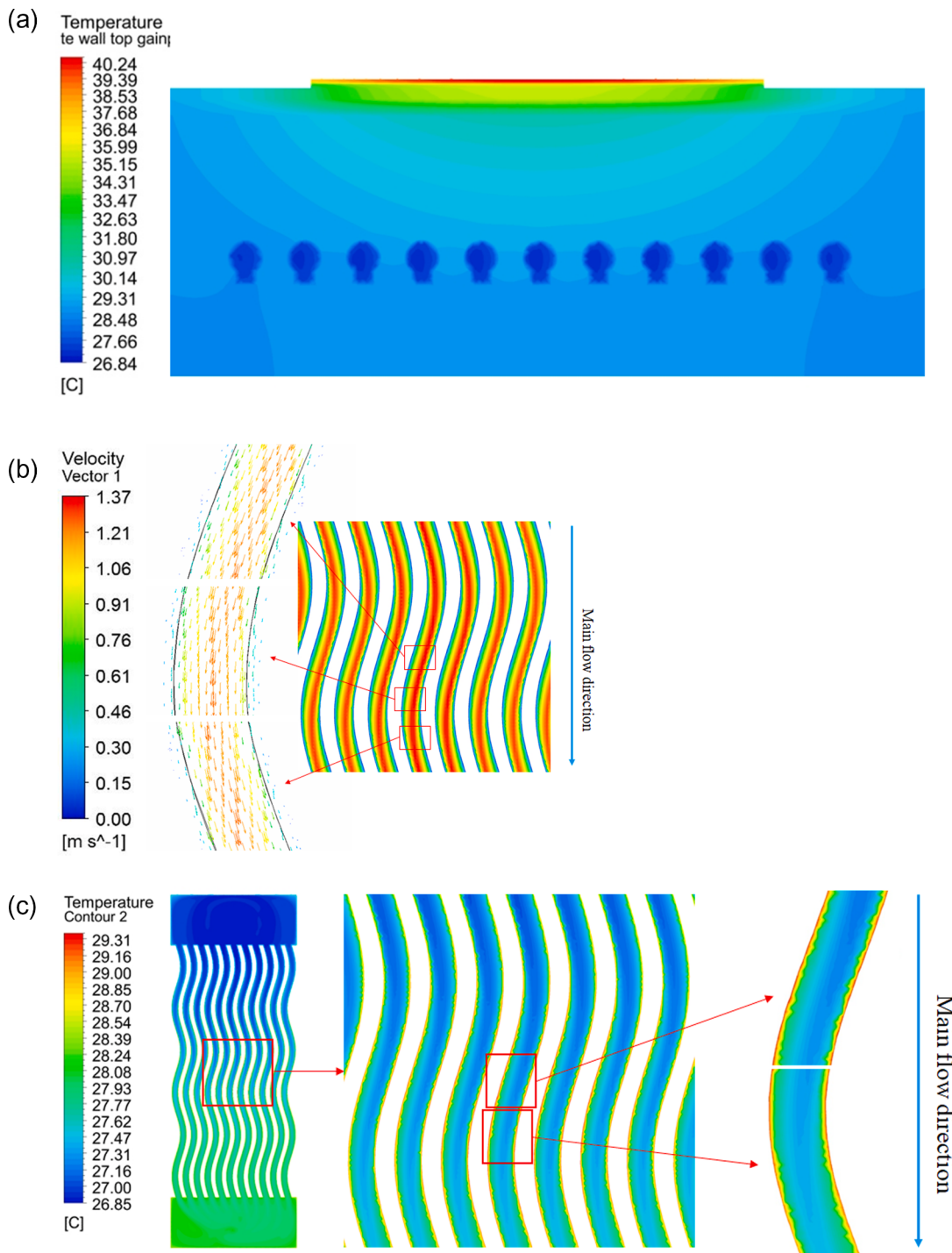


Fig. 12. Simulation results of microchannel heat sinks with serpentine reentrant microchannels: (a)Temperature contours of the cross section of the HCPV cell module; (b) Velocity vectors in serpentine reentrant microchannels; (c) Temperature contours of serpentine reentrant microchannels.

increased. Moreover, the fluid mixing inside the serpentine microchannels was also enhanced at larger flow rates. Therefore, the temperatures of the HCPV cell decreased at larger flow rates. Besides, it can be also noted that the temperatures of PV cell declined rapidly when the flow rate increased from 100 to 200 mL/min, whereas the decrease in temperature tended to be smaller with further increase in the flow rates. Possible reasons for this can be that the improvement in heat transfer performance of microchannel heat sinks tended to be less obvious when the flow rates increased further to large ones. Moreover, the heat extracted by the cooling water in microchannels may tend to increase slightly when the flow rate was larger than a certain value, as pointed

out by Du et al.[41]. The above trend can be also noted from temperature contours of the PV cell in the simulation results of Fig. 16. The high temperature areas of PV cell can be obvious in the smallest flow rate of 100 mL/min, and then tended to reduced with the increase in flow rates. The temperature distribution of PV cell changed slightly when the large flow rates of 400 and 500 mL/min were utilized. On the other hand, the pressure drop across the serpentine reentrant microchannels tended to increase monotonically at larger flow rates. As more pumping power should be supplied to overcome the larger pressure drop at larger flow rates, it seems that the flow rates should be carefully monitored to reach the trade-off between the thermal performance and pumping power.

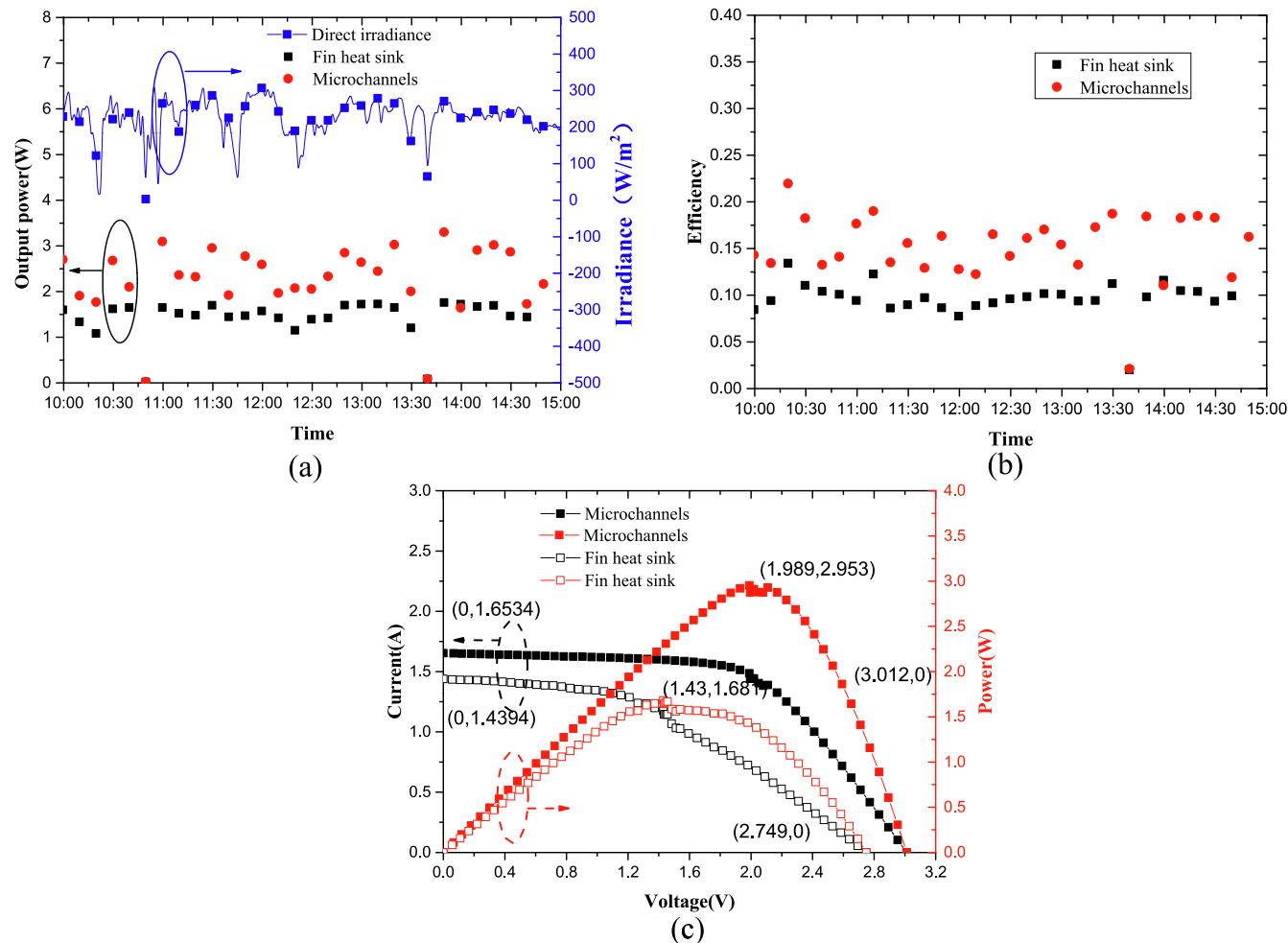


Fig. 13. Electrical performance of HCPV cell modules with both heat sinks:(a) Maximum output power; (b) electrical efficiency; (c) Typical I-V and P-V curves.

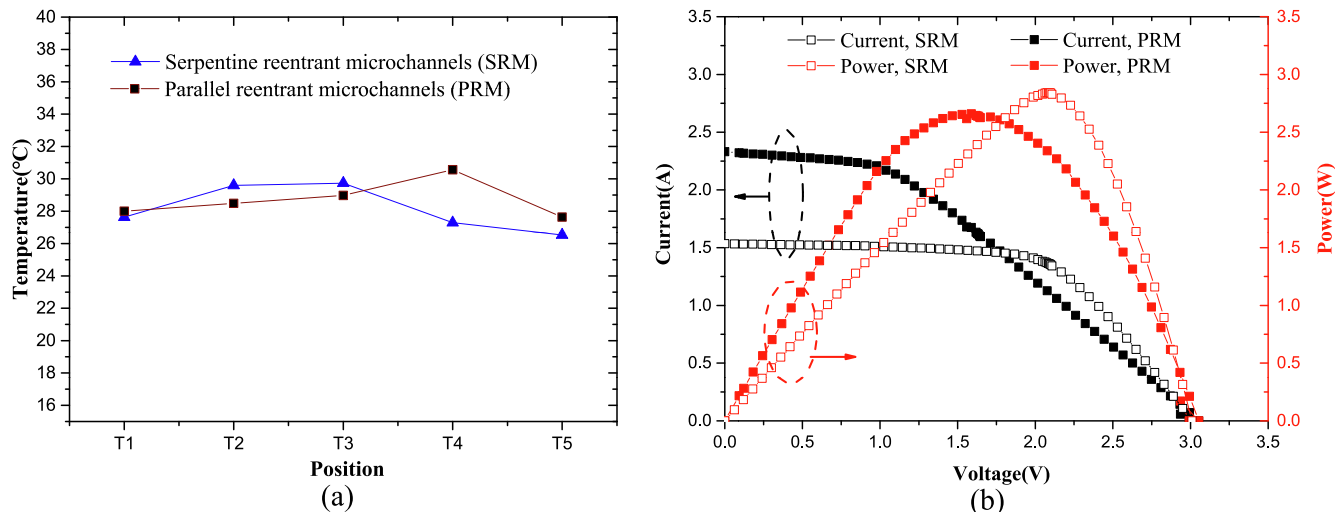


Fig. 14. Comparison of thermal and electrical performance of HCPV cell modules cooled by both serpentine and parallel reentrant microchannels:(a) Temperature distribution on the bottom of the HCPV cooling module; (b) I-V and P-V curves.

Fig. 17 illustrated typical I-V curves and P-V curves of the HCPV cell in different flow rates cases, in which the direct solar radiation was the same of 500 W/m². When the flow rate increases, the maximum output power of the HCPV cell can be noted to increase. The output power increased in general as the flow rate increased. This can be attributed to

that the increase in flow rate induced the decrease of average temperature of HCPV cell, and result in the increase of output electrical performance. From the above, it can be noted that the increase in flow rate contributed to more favorable thermal and output electrical performance of HCPV cell module.

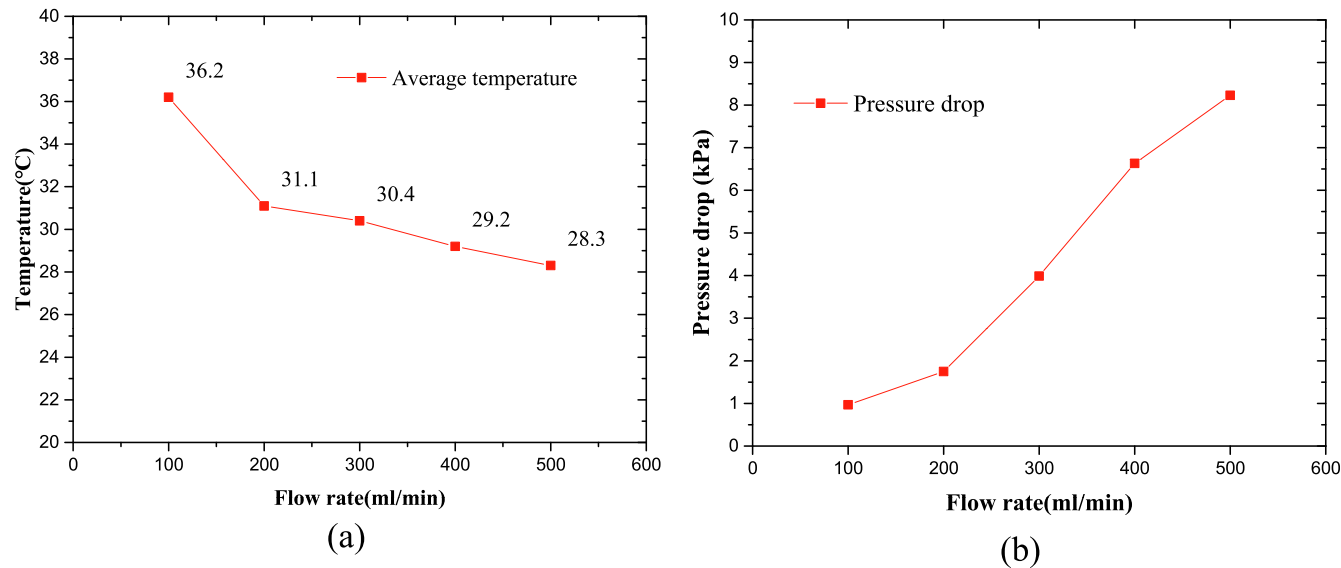


Fig. 15. HCPV cell module with serpentine reentrant microchannels in different flow rates: (a) Average cell temperatures; (b) Pressure drop across the microchannels.

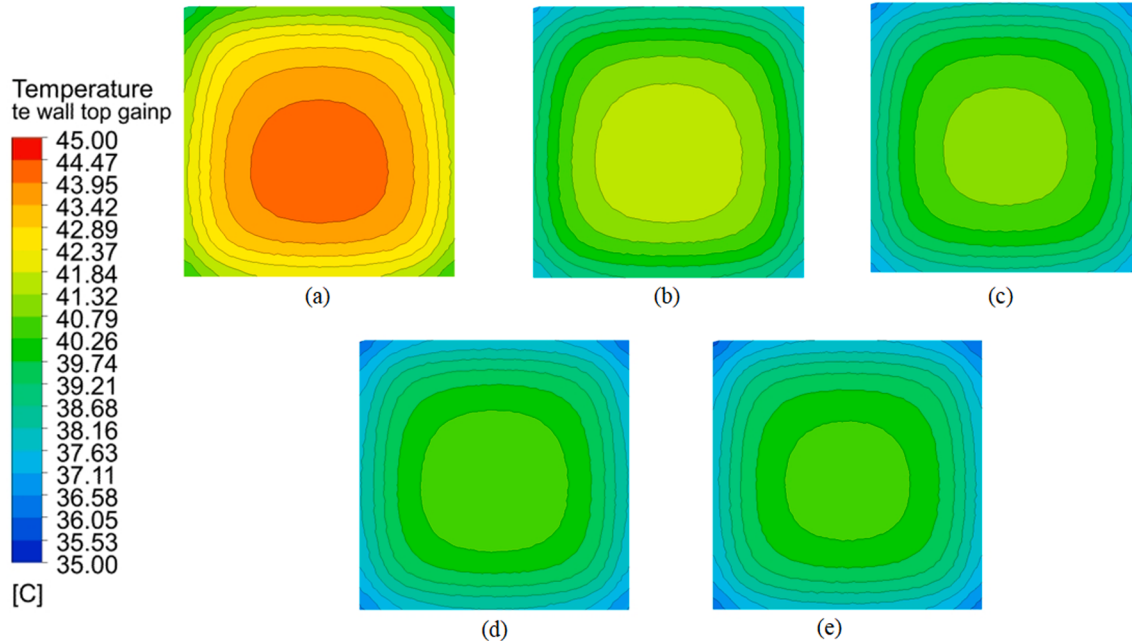


Fig. 16. Temperature contours of the CPV cells in different flow rates: (a) 100 mL/min; (b) 200 mL/min; (c) 300 mL/min; (d) 400 mL/min; (e) 500 mL/min.

4.4. Effect of concentration ratio on the performance of HCPV cell module

Besides of the above tests of the concentration ratio of 1000 \times , another test of concentration ratio of 800 \times were conducted for both HCPV cell module with microchannel and fin heat sink cooling systems by adjusting the incident light area of the Fresnel lens. Fig. 18 shows the output electrical performance of the HCPV cells under the concentration of 800 \times . In this case, the HCPV cells generally presented output power of 3.1–3.2 W with a very small magnitude of fluctuations. By the comparison of Fig. 18 and Fig. 13, the 800 \times case induce more stable and larger output power than the 1000 \times one for the microchannel heat sink cooling module.

To compare the output electrical performance of both concentration ratios cases directly, Fig. 18(b) illustrates a typical I-V and P-V curves of the HCPV cells at the same DNI of 250 W/m². The maximum output

power, short circuit current and open voltage of the HCPV cell under the concentration of 800 \times are 3.2 W, 2.588A and 3.059 V respectively. On the other hand, the maximum output power, short circuit current and open voltage of the HCPV cell under the concentration of 1000 \times are 2.553 W, 1.32A and 2.997 V respectively. Therefore, the small concentration ratio of 800 \times can be found to produce more favorable output electrical performance. Despite that a higher concentration ratio result in more sunlight input on the surface of the cell, it also induced more heat accumulation in the PV cell, which adversely deteriorated the output power of the HCPV cell. Helmers et al. [42] also found that when the concentration ratio increased to high values, the high temperature enhanced the bulk potential barrier effect and lead to more reduction of the triple-junction cell efficiency. Therefore, in the present test ranges, it would be better to select the concentration ratio of 800 \times for the HCPV cell module than that of 1000 \times .

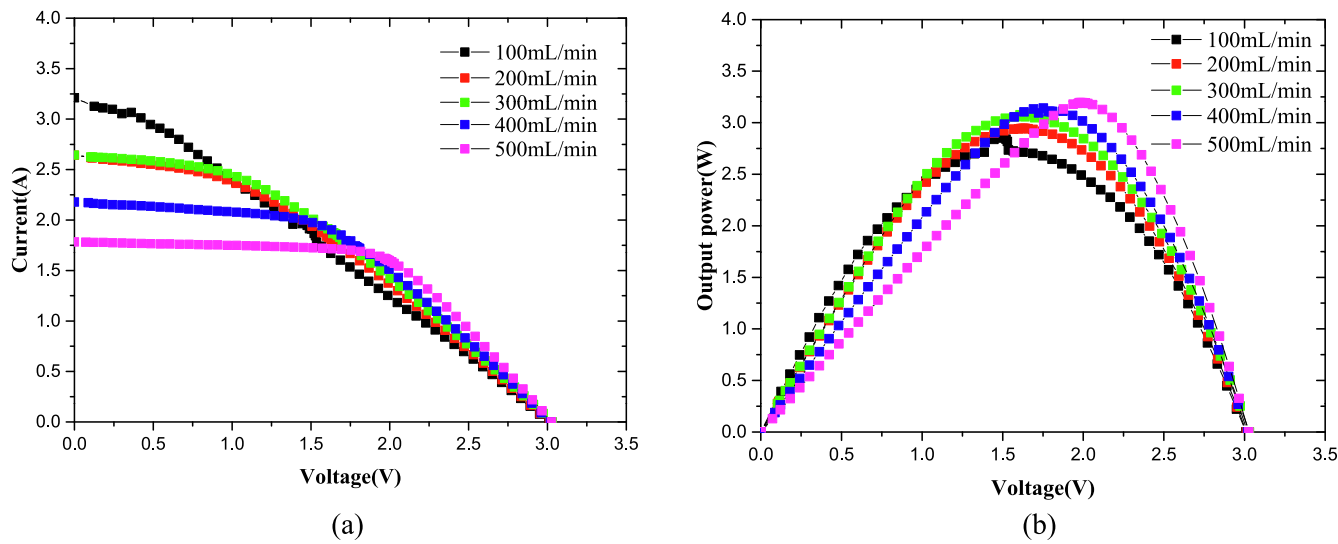


Fig. 17. The output electrical performance in different flow rate (a) I-V curves; (b) P-V curves.

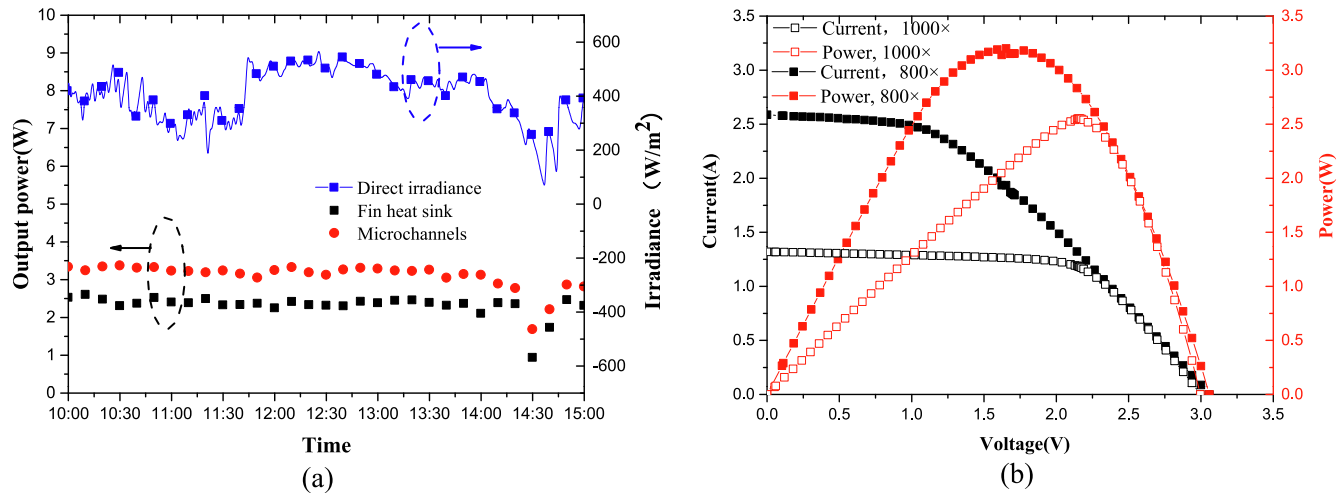


Fig. 18. Electrical performance HCPV cell modules:(a) Maximum output power of the HCPV cells in the concentration ratio of 800×; (b) Comparison of I-V and P-V curves of the HCPV cells between two concentration ratios of 1000 × and 800×.

5. Conclusions

In this study, a unique type of serpentine reentrant microchannels was developed for efficient cooling of HCPV cells. By the comparison of a fin heat sink, the thermal and electrical performance of the HCPV cells with microchannels heat sink were explored by both numerical simulations and outdoor experimental tests. The effects of flow rate and concentration ratio on the performance of the HCPV cell modules with serpentine reentrant microchannels were also investigated. The following conclusions can be drawn:

- (1) By the comparison of the fin heat sink, the serpentine reentrant microchannels reduced the HCPV cell temperatures remarkably. The cell temperatures of HCPV cell module with SRM were found to be within 25–31 °C, which was much smaller than those of 45–63 °C cooled by the fin heat sink. The temperature differences of HCPV cell modules can be also reduced to be less than 4.4 °C for the HCPV cell module with SRM, much smaller than that of 8.1 °C of the fin heat sink. The serpentine reentrant microchannels promoted fluid mixing, and disrupted the normal development of thermal boundary layers. Thus they presented excellent heat

transfer performance and cooling characteristics, and induced much better thermal performance of HCPV cell module.

- (2) The serpentine reentrant microchannels introduced much better output electrical performance of HCPV cell modules than the fin heat sink. It induced a maximum 115% increment in the output power. Moreover, the HCPV cell module with microchannels heat sink generally presented efficiencies of 15–20%, much larger than those of 9–12% of the fin heat sink counterpart.
- (3) By the comparison of parallel reentrant microchannels, the serpentine reentrant microchannels induced smaller maximum and average cell temperatures, and also introduced better electrical performance.
- (4) With the increase in the inlet flow rate of microchannel heat sinks, the average temperature of the HCPV cells decreased monotonically. The output electrical performance of the HCPV cells increased monotonically.
- (5) By the comparison of two concentration ratios of 800 × and 1000 × of HCPV cell modules with SRM, the 800 × case induce more stable and larger output power than the 1000 × one, and was more favorable for the cooling of HCPV cell modules.

As the fabrication of serpentine reentrant microchannels and

packaging methods of microchannel heat sinks can be commonly implemented with low cost, it is believed that the new cooling method with serpentine reentrant microchannels can be promising for the large-scale commercial application.

CRediT authorship contribution statement

Liang Chen: Investigation, Writing – original draft. **Daxiang Deng:** Conceptualization, Supervision, Writing – review & editing, Supervision. **Qixian Ma:** Investigation. **Yingxue Yao:** Methodology. **Xinhai Xu:** Methodology.

Declaration of Competing Interest

The authors declare that they have no known competing financial interests or personal relationships that could have appeared to influence the work reported in this paper.

Acknowledgments

This study is financially supported under the Grants of the National Natural Science Foundation of China (No. 51775464), and was partially supported by Basic research projects of Shenzhen Research & Development Fund (No. JCYJ20200109112808109).

References

- [1] Hasan A, Sarwar J, Shah AH. Concentrated photovoltaic: A review of thermal aspects, challenges and opportunities. *Renew Sustain Energy Rev* 2018;94:835–52.
- [2] Jakhar S, Soni MS, Gakkhar N. Historical and recent development of concentrating photovoltaic cooling technologies. *Renew Sustain Energy Rev* 2016;60:41–59.
- [3] Royne A, Dey C, Mills D. Cooling of photovoltaic cells under concentrated illumination: a critical review. *Sol Energy Mater Sol Cells* 2005;86(4):451–83.
- [4] George M, Pandey AK, Abd Rahim N, Tyagi VV, Shahabuddin S, Saidur R. Concentrated photovoltaic thermal systems: A component-by-component view on the developments in the design, heat transfer medium and applications. *Energy Convers Manage* 2019;186:15–41.
- [5] Natarajan SK, Mallick TK, Katz M, Weingartner S. Numerical investigations of solar cell temperature for photovoltaic concentrator system with and without passive cooling arrangements. *Int J Thermal Sci* 2011;50(12):2514–21.
- [6] Theristis M, Fernández EF, Sumner M, O'Donovan TS. Multiphysics modelling and experimental validation of high concentration photovoltaic modules. *Energy Convers Manage* 2017;139:122–34.
- [7] Zhu Li, Wang Y, Fang Z, Sun Y, Huang Q. An effective heat dissipation method for densely packed solar cells under high concentrations. *Sol Energy Mater Sol Cells* 2010;94(2):133–40.
- [8] Xin G, Wang Y, Sun Y, Huang Q, Zhu Li. Experimental study of liquid-immersion III-V multi-junction solar cells with dimethyl silicon oil under high concentrations. *Energy Convers Manage* 2015;94:169–77.
- [9] Ma T, Yang H, Zhang Y, Lu L, Wang X. Using phase change materials in photovoltaic systems for thermal regulation and electrical efficiency improvement: A review and outlook. *Renew Sustain Energy Rev* 2015;43:1273–84.
- [10] Rabie R, Emam M, Ookawara S, Ahmed M. Thermal management of concentrator photovoltaic systems using new configurations of phase change material heat sinks. *Sol Energy* 2019;183:632–52.
- [11] Wang Z, Zhang H, Wen D, Zhao W, Zhou Z. Characterization of the InGaP/InGaAs/Ge triple-junction solar cell with a two-stage dish-style concentration system. *Energy Convers Manage* 2013;76:177–84.
- [12] Royne A, Dey CJ. Design of a jet impingement cooling device for densely packed PV cells under high concentration. *Sol Energy* 2007;81(8):1014–24.
- [13] Rahimi M, Valeh-e-Sheyda P, Parsamoghadam MA, Masahi MM, Alsairafi AA. Design of a self-adjusted jet impingement system for cooling of photovoltaic cells. *Energy Convers Manage* 2014;83:48–57.
- [14] Gilmore N, Timchenko V, Menicas C. Microchannel cooling of concentrator photovoltaics: A review. *Renew Sustain Energy Rev* 2018;90:1041–59.
- [15] Riera S, Barrau J, Omri M, Fréchette LG, Rosell JI. Stepwise varying width microchannel cooling device for uniform wall temperature: Experimental and numerical study. *Appl Therm Eng* 2015;78:30–8.
- [16] Abo-Zahhad EM, Ookawara S, Radwand A, El-Shazly AH, Elkady MF. Numerical analyses of hybrid jet impingement microchannel cooling device for thermal management of high concentrator triple-junction solar cell. *Appl Energy* 2019;253:113538.
- [17] Deng D, Wan W, Qin Y, Zhang J, Chu X. Flow boiling enhancement of structured microchannels with micro pin fins. *Int J Heat Mass Transf* 2017;105:338–49.
- [18] Deng D, Zeng L, Sun W. A review on flow boiling enhancement and fabrication of enhanced microchannels of microchannel heat sinks. *Int J Heat Mass Transf* 2021;175:121332. <https://doi.org/10.1016/j.ijheatmasstransfer.2021.121332>.
- [19] Agrawal S, Tiwari A. Experimental validation of glazed hybrid micro-channel solar cell thermal tile. *Sol Energy* 2011;85(11):3046–56.
- [20] Rahimi M, Karimi E, Asadi M, Valeh-e-Sheyda P. Heat transfer enhancement in a PV cell using Boehmite nanofluid. *Int Comm Heat Mass Transf* 2013;43:131–7.
- [21] Yang K, Zuo C. A novel multi-layer manifold microchannel cooling system for concentrating photovoltaic cells. *Energy Convers Manage* 2015;89:214–21.
- [22] Ali AYM, Abo-Zahhad EM, Elkady MF, Ookawara S, El-Shazly AH, Radwan A. Temperature uniformity enhancement of densely packed high concentrator photovoltaic module using four quadrants microchannel heat sink. *Sol Energy* 2020;202:446–64.
- [23] Radwan A, Ookawara S, Moria S, Ahmed M. Uniform cooling for concentrator photovoltaic cells and electronic chips by forced convective boiling in 3D-printed monolithic double-layer microchannel heat sink. *Energy Convers Manage* 2018;166:356–71.
- [24] Al Siyabi I, Shanks K, Mallick T, Sundaram S. Indoor and outdoor characterization of concentrating photovoltaic attached to multi-layered microchannel heat sink. *Sol Energy* 2020;202:55–72.
- [25] Hong S, Zhang B, Dang C, Hihara E. Development of two-phase flow microchannel heat sink applied to solar-tracking high-concentration photovoltaic thermal hybrid system. *Energy* 2020;212:118739.
- [26] Sui Y, Lee PS, Teo CJ. An experimental study of flow friction and heat transfer in wavy microchannels with rectangular cross section. *Int J Thermal Sci* 2011;50(12):2473–82.
- [27] Khoshvaght-Aliabadi M, Sahamiyan M, Hesampour M, Sartipzadeh O. Experimental study on cooling performance of sinusoidal-wavy minichannel heat sink. *Appl Therm Eng* 2016;92:50–61.
- [28] Al-Neama AF, Kapur N, Summers J, Thompson HM. An experimental and numerical investigation of chevron fin structures in serpentine minichannel heat sinks. *Appl Therm Eng* 2017;116:709–23.
- [29] Xia G, Zhai Y, Cui Z. Numerical investigation of thermal enhancement in a micro heat sink with fan-shaped reentrant cavities and internal ribs. *Appl Therm Eng* 2013;58(1-2):52–60.
- [30] Chai L, Xia G, Wang L, Zhou M, Cui Z. Heat transfer enhancement in microchannel heat sinks with periodic expansion constriction cross-sections. *Int J Heat Mass Transf* 2013;62:741–51.
- [31] Deng D, Wan W, Tang Y, Shao H, Huang Y. Experimental and numerical study of thermal enhancement in reentrant copper microchannels. *Int J Heat Mass Transf* 2015;91:656–70.
- [32] Yin E, Li Q, Li D, Xuan Y. Experimental investigation on effects of thermal resistances on a photovoltaic-thermoelectric system integrated with phase change materials. *Energy* 2019;169:172–85.
- [33] Taylor JR. An Introduction to Error Analysis, second ed. University Science Books 1997.
- [34] Aldossary A, Mahmoud S, AL-Dadah R. Technical feasibility study of passive and active cooling for concentrator PV in harsh environment. *Appl Therm Eng* 2016;100:490–500.
- [35] Dong J, Zhuang X, Xu X, Miao Z, Xu B. Numerical analysis of a multi-channel active cooling system for densely packed concentrating photovoltaic cells. *Energy Convers Manage* 2018;161:172–81.
- [36] Holman JP. Heat transfer, 9th ed. McGraw-Hill; 2002. p. 225–226.
- [37] Abo-Zahhad E, Ookawara S, Radwand A, El-Shazly AH, Elkady MF. Numerical analyses of hybrid jet impingement microchannel cooling device for thermal management of high concentrator triple-junction solar cell. *Appl Energy* 2019;253:113538.
- [38] ANSYS Fluent 16.0 Theory Guide, ANSYS Inc., USA.
- [39] Cui T, Xuan Y, Yin E, Li Q, Li D. Experimental investigation on potential of a concentrated photovoltaic-thermoelectric system with phase change materials. *Energy* 2017;122:94–102.
- [40] Du D, Darkwa Jo, Kokogiannakis G. Thermal management systems for Photovoltaics (PV) installations: A critical review. *Sol Energy* 2013;97:238–54.
- [41] Du B, Hu E, Kolhe M. Performance analysis of water cooled concentrated/photovoltaic (CPV) system. *Renew Sustain Energy Rev* 2012;16:6732–6.
- [42] Helmers H, Schachter M, Bett AW. Influence of temperature and irradiance on triple-junction solar subcells. *Sol Energy Mater Sol Cells* 2013;116:144–52.